Progress In Electromagnetics Research C, Vol. 94, 1–12, 2019

Measurement of the Influence of Antennas on Radio Signal Propagation in Underground Mines and Tunnels

Ronald Jacksha[1, *], Chenming Zhou[2], and Carl Sunderman[1]

Abstract—This paper reports the influence of antennas on radio signal propagation in tunnels and underground mines. Radio signal propagation measurement results in a concrete tunnel and underground mines using antenna types with various radiation patterns, i.e., omnidirectional, Yagi, patch, and circular, are reported. Extensive measurements were taken in various scenarios which include vertical, horizontal, and circular polarization for line-of-sight (LoS) radio signal propagation at four frequencies (455, 915, 2450, and 5800 MHz) that are common to many voice and data transport radio systems used in underground mines. The results show that antenna pattern has a strong influence on the uniformity of radio signal propagation gain in the near zone and typically does not significantly influence behavior in the far zone, except for a constant gain offset.

1. INTRODUCTION

Radio frequency (RF)-based wireless systems operating in the ultra-high frequency (UHF) and super-high frequency (SHF) bands are becoming commonplace in underground mines. These wireless systems provide voice communications, data transport, miner tracking, proximity detection, and environmental monitoring and control. Understanding RF signal propagation in underground mines is critical to the optimal performance and reliability of these wireless systems and, as a result, will contribute to enhancing overall miner safety and health.

While RF signal propagation in underground mines and tunnels has been studied for decades [1–10], most of the prior studies assume omnidirectional antennas for both the transmitter and the receiver, and the influence of antenna pattern on tunnel RF signal propagation has not been investigated. Particularly, RF signal propagation measurements in underground mines and tunnels have primarily been performed using omnidirectional antennas [2, 10–12]. In practice, however, wireless systems installed in underground mines often use other types of antennas that could have distinctly different RF signal propagation characteristics. A recent study reported results of RF signal propagation measurements in a small concrete tunnel using various types of antennas [13]. This paper expands on that study by reporting RF signal propagation measurements conducted in the more complex environments of underground mines, using four different antenna types (omnidirectional, Yagi, patch, and circular antennas) that were operated at 455, 915, 2450, and 5800 MHz and at three polarizations (horizontal, vertical, and circular).

2. MODELING RADIO SIGNAL PROPAGATION WITH ANTENNA PATTERNS INCLUDED

Figure 1 illustrates the cross-sectional view of a straight rectangular tunnel.

Received 25 March 2019, Accepted 26 June 2019, Scheduled 7 July 2019
* Corresponding author: Ronald Jacksha (gyt6@cdc.gov).
[1] CDC/NIOSH, Spokane, WA 99207, USA. [2] CDC/NIOSH, Pittsburgh, PA 15236, USA.

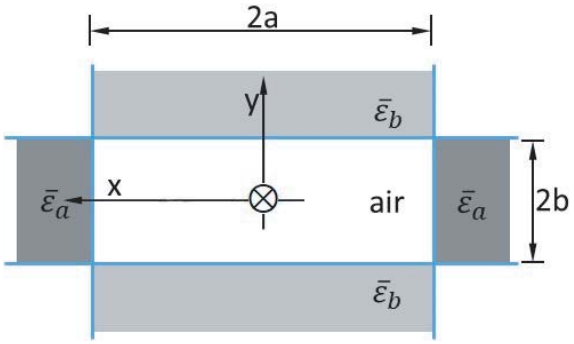

Figure 1. Cross-sectional view of the tunnel.

In this illustration, the width and height of the tunnel are $2a$ and $2b$, respectively. Let $T(x_0, y_0, 0)$ and $R(x, y, z)$ represent the location of the transmitter and receiver. $f_t\left(\widehat{\theta}_t, \widehat{\varphi}_t\right)$, $f_r\left(\widehat{\theta}_r, \widehat{\varphi}_r\right)$ are radiation patterns for the transmitter and receiver antenna, respectively. Without loss of generality, we also assume the source is vertically polarized. Horizontal polarization results can be derived in a similar manner. Based on the ray tracing theory, the received electric field can be obtained by summing the scalar electric fields of the rays from all the images of the source as [14]:

$$E_r(x, y, z) = E_t \sum_{m=-\infty}^{+\infty} \sum_{n=-\infty}^{+\infty} \frac{e^{-jkr_{m,n}}}{r_{m,n}} f_t\left(\widehat{\theta}_{m,n}, \widehat{\varphi}_{m,n}\right) f_r\left(\widehat{\theta}_{m,n}, \widehat{\varphi}_{m,n}\right) \rho_{\perp}^{|m|} \rho_{//}^{|n|} \tag{1}$$

where E_t is the magnitude of the transmitted electric field; k is the wave number in the waveguide (free space); and $r_{m,n}$ is the distance between the receiver and the image $I_{m,n}$ and is given by [1, 14]:

$$r_{m,n} = \sqrt{(2ma + (-1)^m x_0 - x)^2 + (2nb + (-1)^n y_0 - y)^2 + z^2} \tag{2}$$

$\rho_{\perp,//}$ represent the perpendicular and parallel reflection coefficients, respectively, and can be readily calculated as [15]:

$$\begin{aligned} \rho_{\perp} &= \frac{\cos\theta_{m,n} - \sqrt{\bar{\varepsilon}_a - 1 + \cos^2\theta_{m,n}}}{\cos\theta_{m,n} + \sqrt{\bar{\varepsilon}_a - 1 + \cos^2\theta_{m,n}}} \\ \rho_{//} &= \frac{\cos\varphi_{m,n} - \sqrt{\bar{\varepsilon}_b - 1 + \cos^2\varphi_{m,n}}\Big/\bar{\varepsilon}_b}{\cos\varphi_{m,n} + \sqrt{\bar{\varepsilon}_b - 1 + \cos^2\varphi_{m,n}}\Big/\bar{\varepsilon}_b} \end{aligned} \tag{3}$$

where $\bar{\varepsilon}_{a,b} = [\varepsilon_{a,b} - j\sigma_{a,b}/(2\pi f)]/\varepsilon_0$ denote the complex relative permittivities of the vertical and horizontal reflection surfaces. $\theta_{\perp,//}$ are the corresponding angles of incidence relative to the normal to the reflecting surface and are given by:

$$\begin{aligned} \cos\theta_{m,n} &= \frac{|2ma + (-1)^m x_0 - x|}{r_{m,n}} \\ \cos\varphi_{m,n} &= \frac{|2nb + (-1)^n y_0 - y|}{r_{m,n}} \end{aligned} \tag{4}$$

It has been shown in [10] that in the far zone (see Section 5 for discussion of the "far zone") both $\theta_{m,n}$ and $\varphi_{m,n}$ are very small so that

$$\begin{aligned} f_t\left(\widehat{\theta}_{m,n}, \widehat{\varphi}_{m,n}\right) &\approx G_t \\ f_r\left(\widehat{\theta}_{m,n}, \widehat{\varphi}_{m,n}\right) &\approx G_r \end{aligned} \tag{5}$$

where G_t and G_r represent transmitter and receiver antenna gains respectively.

Substituting Eq. (5) into Eq. (1) yields

$$E_r(x,y,z) \approx G_t G_r E_t \sum_{m=-\infty}^{+\infty} \sum_{n=-\infty}^{+\infty} \frac{e^{-jkr_{m,n}}}{r_{m,n}} \rho_{\perp}^{|m|} \rho_{//}^{|n|} \quad \text{for large } z \tag{6}$$

For omnidirectional antennas where $G_t = G_r = 1$, Eq. (6) reduces to

$$E_r(x,y,z) = E_t \sum_{m=-\infty}^{+\infty} \sum_{n=-\infty}^{+\infty} \frac{e^{-jkr_{m,n}}}{r_{m,n}} \rho_{\perp}^{|m|} \rho_{//}^{|n|} \tag{7}$$

A comparison of Eqs. (7) and (6) shows that in the far zone where z is sufficiently large, the received power is not significantly affected by the antenna patterns, except for a difference of a constant gain (i.e., $G_t G_r$) which is determined by the antenna patterns shown in Eq. (5), and the alignment of the two antennas. In the near zone (see Section 5 for discussion of the "near zone") where z is small, the contribution from the transmitter and receiver antenna patterns is highly dependent on angles of each ray and thus has a significant influence on the received power.

3. MEASUREMENT SYSTEM AND CONFIGURATION

3.1. Measurement System

The measurement system was composed of two assemblies: a stationary transmitter (Tx) and a mobile receiver (Rx). The transmitter consisted of an RF signal source connected to an antenna using a coaxial cable. The receiver consisted of a data logging spectrum analyzer connected to an antenna through coaxial cable with both the analyzer and antenna being mounted to a mobile cart. A full description of the measurement system and test methodology can be found in [10].

3.2. Measurement Configuration

The spectrum analyzer was centered at the frequency being measured with a frequency span of 2 kHz, a resolution bandwidth of 100 Hz, and the preamp disabled. These settings allowed for displayed average noise levels of approximately −120 dBm at 455 and 915 MHz and −115 dBm at 2450 and 5800 MHz. The spectrum analyzer was configured to perform channel power measurements in a 1-kHz bandwidth using three averages for each reading. The signal generator was configured to produce a continuous

Table 1. Antennas used for measurements.

Frequency	Type	Manufacturer	Model	Gain	Polarization	Beamwidth
455 MHz	Omni	Laird	FG4500	2.15 dBi	Linear	Az-360°/El-70°
	Yagi	Laird	Y4505	11.3 dBi	Linear	Az-72°/El-57°
915 MHz	Omni	Laird	FG8960	2.15 dBi	Linear	Az-360°/El-110°
	Yagi	Laird	Y8966	11.2 dBi	Linear	Az-56°/El-52°
	Flat Patch	L-Com	HG908P	8 dBi	Linear	Az-75°/El-65°
	Flat Patch	L-Com	HG908PCR	8 dBiC	RH Circular	Az-65°/El-65°
2450 MHz	Omni	Laird	FG24005	5 dBi	Linear	Az-360°/El-110°
	Yagi	Laird	YE240015	14.5 dBi	Linear	Az-20°/El-18°
	Flat Patch	L-Com	HG2409P	8 dBi	Linear	Az-75°/El-65°
	Flat Patch	L-Com	HG908PCR	8 dBiC	RH Circular	Az-65°/El-65°
5800 MHz	Omni	SuperPass	SPDJ4O	6.5 dBi	Linear	Az-360°/El-24°
	Yagi	Terrawave	T58150Y13602	15 dBi	Linear	Az-25°/El-24°
	Flat Patch	L-Com	HG5158P	8 dBi	Linear	Az-75°/El-60°
	Flat Patch	L-Com	HG4958-07PCR	8 dBiC	RH Circular	Az-65°/El-65°

wave signal at 0 dBm as measured by a power meter at the antenna end of the coaxial interconnect cable.

Measurements were performed at the four frequencies of interest — 455, 915, 2450, and 5800 MHz — using an antenna height of 1.2 m for both Tx and Rx antennas. At each frequency of interest, vertical and horizontal co-polarized reference measurements were first performed using omnidirectional Tx and Rx antennas. For subsequent co-polarized vertical and horizontal measurements, the Tx was changed to a directional antenna while the Rx antenna remained omnidirectional. To change between vertical and horizontal co-polarization, both Tx and Rx antennas were simply rotated 90°. In the case of the circular polarization, the Tx antennas remained fixed and the Rx antennas were rotated to achieve vertical or horizontal polarization.

The antennas, manufacturers, and specifications are listed in Table 1. Representative samples of the antennas are shown in Fig. 2.

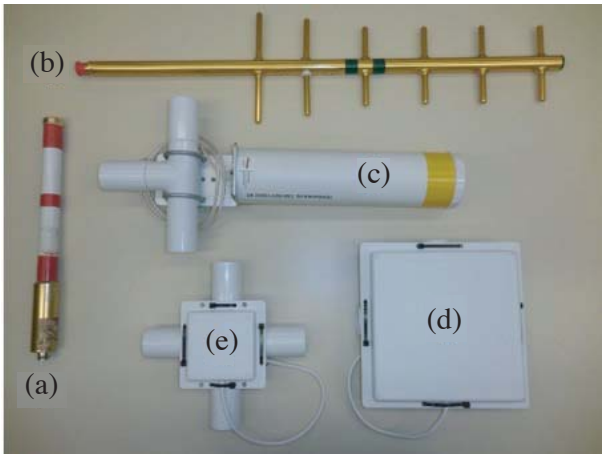

Figure 2. Antennas: (a) 2450 MHz omnidirectional, (b) 915 MHz Yagi, (c) 2450 MHz Yagi, (d) 925 MHz patch, (e) 5800 MHz circular.

4. TEST SITES

RF signal propagation measurements were performed in three underground mine/tunnel environments: a small concrete tunnel, a high-seam western United States coal mine entry, and a research coal mine entry.

The concrete tunnel was the 900 Gallery located within the Grand Coulee Dam in Washington State. The gallery dimensions were 1.8 m wide by 2.4 m tall with an arched ceiling beginning 1.5 m up the side of the wall. The walls were very smooth with a single conduit pipe running along the ceiling. A picture of the 900 Gallery is shown in Fig. 3.

The width of the western high-seam coal mine's entry varied from 5.6 m to 5.9 m, and the height varied from 2.7 m to 3.4 m. The walls and floor were heavily rock dusted and the ceiling was covered with extensive ground control measures consisting of roof bolts, steel mesh, and support cables. A picture of the entry is shown in Fig. 4.

The research coal mine was the National Institute for Occupational Safety and Health's (NIOSH's) Bruceton Experimental Mine located south of Pittsburgh, Pennsylvania. Measurements were conducted in the Main entry which had an average width of 4 m and an average height of 2 m. Many metallic conductors were present: steel beams on the ceilings and walls, various electric and communications cables on both walls, and rails on the floor. A picture of the Main entry is shown in Fig. 5.

Figure 3. Grand Coulee Dam 900 gallery.

Figure 4. Western high seam coal mine entry.

Figure 5. Bruceton experimental mine main entry.

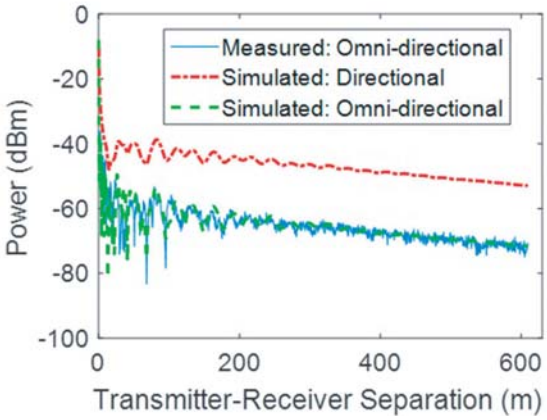

Figure 6. Evaluation of the influence of antenna pattern based on ray tracing theory. The measured result for the omni-directional antenna case is plotted for reference.

5. RESULTS AND DISCUSSION

Figure 6 shows a comparison of simulated propagation loss for different antennas in the 900 Gallery of Grand Coulee Dam, assuming the source is vertically polarized with a frequency of 2.45 GHz. The measured propagation loss with an omni-directional antenna is also plotted for reference. More details about the comparison between the simulated and measured results for different polarizations at a variety of frequencies can be found in [14]. In Fig. 6, the following Gaussian function has been manually introduced to represent the main lobe of the antenna pattern (for both transmitter and receiver antennas):

$$f_t\left(\widehat{\theta}_t, \widehat{\varphi}_t\right) = \sqrt{G_0 \exp\left[-2.773\left(\left(\frac{\frac{\pi}{2} - \theta_{m,n}}{w_b}\right)^2 + \left(\frac{\frac{\pi}{2} - \varphi_{m,n}}{w_b}\right)^2\right)\right]} \tag{8}$$

where G_0 is a gain constant, and w_b is the 3-dB beam width of the main lobe. Particularly, $G_0 = 10$ and $w_b = 10$ degrees have been used to calculate the simulated propagation loss with directional antennas

in Fig. 6. As expected, it can be found from Fig. 6 that the influence of antenna pattern is primarily a constant power offset determined by the gain of the transmitter and receiver antennas. It should also be noted that the simulated and the measured propagation loss results for the omnidirectional antenna case show a very good agreement.

Previous research has shown that there are near and far zone regions of line-of-sight RF propagation in underground mines and tunnels [10, 16–20]. In the near zone signal power fluctuates widely while in the far zone the signal attenuates linearly with distance. The point separating the near and far zones is known as the Fresnel zone breaking point [16–20]. The breaking point is a unique feature of tunnel propagation and is generally related to the signal wavelength and tunnel dimensions. As shown in the modeling section of this paper (Section 2), the ray tracing modeling predicts that antenna pattern would have a strong influence on the uniformity of RF signal gain in the near zone and does not significantly influence the far zone with the exception of a constant gain offset. For these reasons, measurement results for the near and far zones were analyzed separately. Fig. 7 shows an example of the near and far zones of RF propagation in a concrete tunnel measuring 1.8 m wide by 2.4 m high.

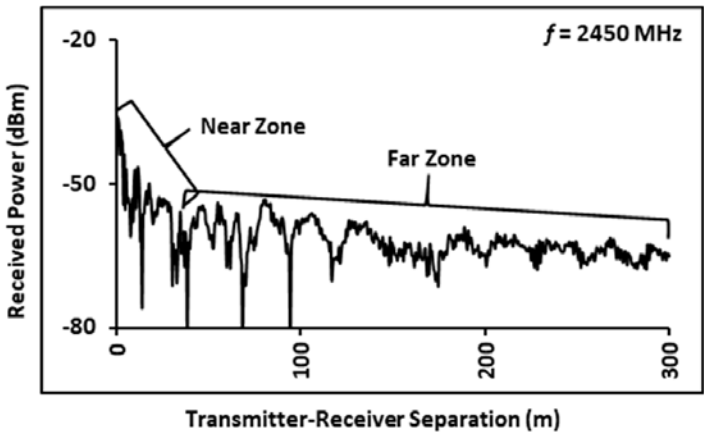

Figure 7. Near and far zones of line-of-sight RF propagation in a concrete tunnel.

5.1. Near Zone of RF Signal Propagation

Measurement results support the ray tracing modeling prediction that antenna pattern has a strong influence on the uniformity of RF signal gain in the near zone of propagation. While the influence

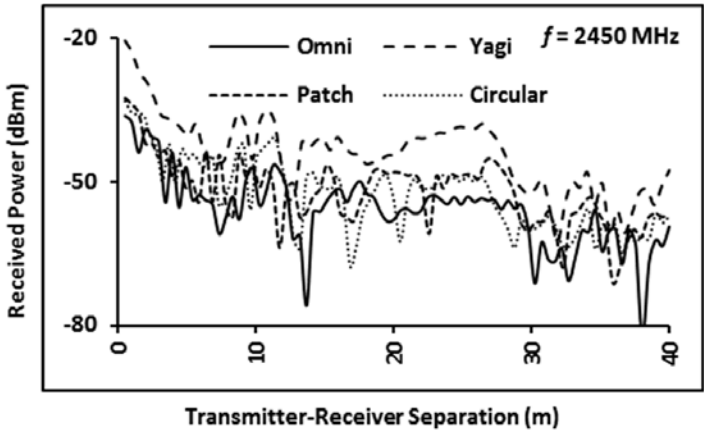

Figure 8. Evaluation of the influence of antenna pattern in the near zone of RF propagation.

is strong, it appears there is no reasonably viable way to correlate differences in RF propagation measurement results between antennas in the near zone with any level of accuracy. Fig. 8 shows a typical result of the measurement of the influence of antenna pattern on RF propagation in the near zone.

5.2. Far Zone of RF Signal Propagation

Measurement results for the influence of antenna pattern on the far zone of RF propagation were evaluated by comparing differences in RF signal propagation attenuation slopes and RF signal propagation gains.

Signal attenuation slopes, based on a method of linear regression fitting, were estimated from a point beyond the near zone — 20 m for 455 MHz, 40 m for 915 and 2450 MHz, and 80 m for 5800 MHz — to the end of the far zone of measured RF propagation for each frequency, antenna, and polarization combination. Attenuation slope differences were then calculated for similar frequency, antenna, and polarization combinations using the omnidirectional antenna at each frequency and polarization as a reference. Fig. 9 shows a comparison of signal attenuation slopes with linear regression fit trend lines and the estimated signal gain for omnidirectional and Yagi antennas at 2450 MHz. The method for estimating signal gain is described later in this section.

Attenuation slope comparisons predominantly supported the ray tracing modeling prediction that

Table 2. Summary of estimated RF signal propagation attenuation slopes.

Frequency/ Far Zone	Antenna Parameters		Grand Coulee Dam		Western Coal Mine		Experimental Mine	
			Attenuation Slope		Attenuation Slope		Attenuation Slope	
	Pol.	Type	dB/100 m	Diff. (dB)	dB/100 m	Diff. (dB)	dB/100 m	Diff. (dB)
455 MHz > 20 m	TxV-RxV	Omni	55.52	Ref	24.00	Ref	71.94	Ref
		Yagi	56.48	-0.96	25.20	-1.20	68.81	3.13
	TxH-RxH	Omni	63.50	Ref	11.95	Ref	35.81	Ref
		Yagi	76.43	-12.93	11.42	0.53	35.76	0.05
915 MHz > 40 m	TxV/C-RxV	Omni	14.54	Ref	11.46	Ref	22.75	Ref
		Yagi	14.06	0.48	11.61	-0.15	22.53	0.22
		Patch	14.19	0.35	11.38	0.08	22.37	0.38
		Circular	14.39	0.15	10.60	0.86	16.02	6.73
	TxH/C-RxH	Omni	24.63	Ref	7.26	Ref	11.09	Ref
		Yagi	24.95	-0.32	8.40	-1.14	11.19	-0.10
		Patch	25.24	-0.61	7.67	-0.41	11.00	0.09
		Circular	20.92	3.71	7.57	-0.31	11.17	-0.08
2450 MHz > 40 m	TxV/C-RxV	Omni	2.38	Ref	7.11	Ref	5.75	Ref
		Yagi	2.41	-0.03	6.88	0.23	5.46	0.29
		Patch	2.44	-0.06	7.16	-0.05	5.62	0.13
		Circular	2.58	-0.20	6.44	0.67	5.53	0.22
	TxH/C-RxH	Omni	4.09	Ref	8.83	Ref	5.78	Ref
		Yagi	4.13	-0.04	8.39	0.44	5.66	0.12
		Patch	4.20	-0.11	8.73	0.10	6.10	-0.32
		Circular	4.12	-0.03	5.75	3.08	5.08	0.70
5800 MHz > 80 m	TxV/C-RxV	Omni	0.91	Ref	5.12	Ref	6.59	Ref
		Yagi	2.26	-1.35	5.21	-0.09	7.00	-0.41
		Patch	1.92	-1.01	3.05	2.07	6.81	-0.22
		Circular	2.00	-1.09	3.57	1.55	6.60	-0.01
	TxH/C-RxH	Omni	2.07	Ref	6.40	Ref	7.84	Ref
		Yagi	1.92	0.15	5.17	1.23	7.08	0.76
		Patch	1.13	0.94	5.54	0.86	8.31	-0.47
		Circular	1.34	0.73	12.25	-5.85	6.20	1.64

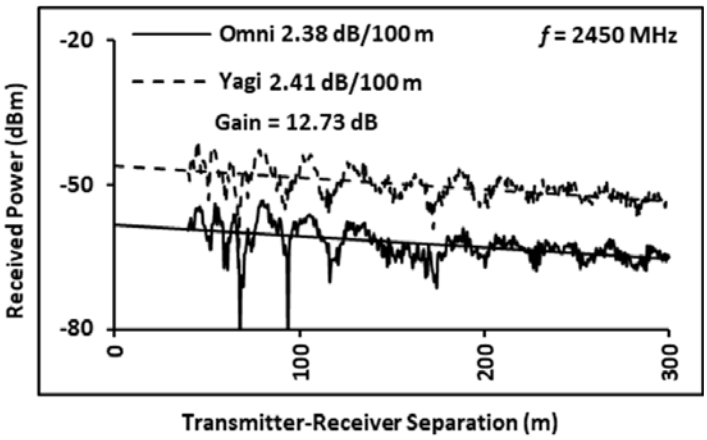

Figure 9. Evaluation of the influence of antenna pattern in the far zone of RF propagation.

antenna pattern does not significantly influence the far zone of propagation with the exception of a constant gain offset. As is shown in Table 2, differences in RF signal propagation attenuation slopes for different antennas were generally less than 1.5 dB/100 m. (See Section 6 for a full discussion of the data in Table 2.) However, under a narrow set of circumstances, slopes differed from 3 dB to greater than 12 dB. These circumstances involved the influences of differing levels of cross polarization-isolation, discussed below, for linear polarized and circular polarized antennas, in small dimension tunnels.

Linear polarized antennas are not perfect radiators, or receivers, of RF signals. Aside from the primary polarization, some amount of RF signal is transmitted, and received, in the orthogonal- or cross-polarization. The ability of an antenna to maintain transmit or receive polarization integrity is referred to as cross polarization-isolation [21]. The amount of an antenna's cross polarization-isolation can have a substantial influence on RF propagation in smaller-dimension tunnels with significant height to width ratios which act as lossy waveguides [2, 10, 14].

This was the case in the 900 Gallery of the Grand Coulee Dam at 455 MHz. A comparison of signal attenuation slope data for horizontally polarized Yagi and omnidirectional antennas showed that they differed by more than 12 dB (Fig. 10).

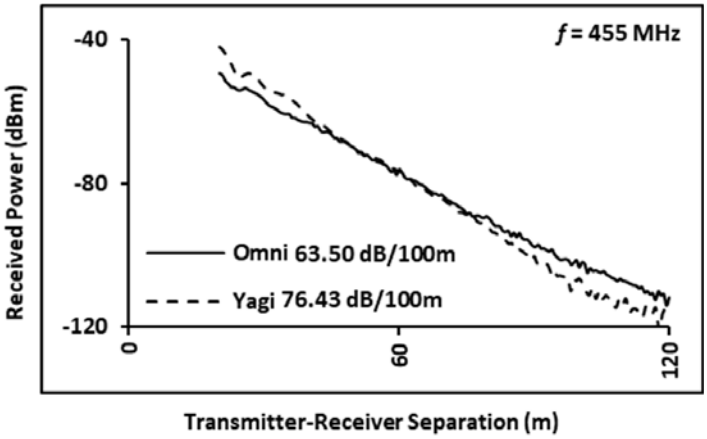

Figure 10. Influence of differences in antenna cross polarization-isolation.

Unlike linearly polarized antennas, which are designed to principally transmit or receive a signal in a single plane, circular polarized antennas are designed to transmit or receive a signal which rotates equally through orthogonal planes of polarization [22, 23]. A circular polarized antenna can also have a

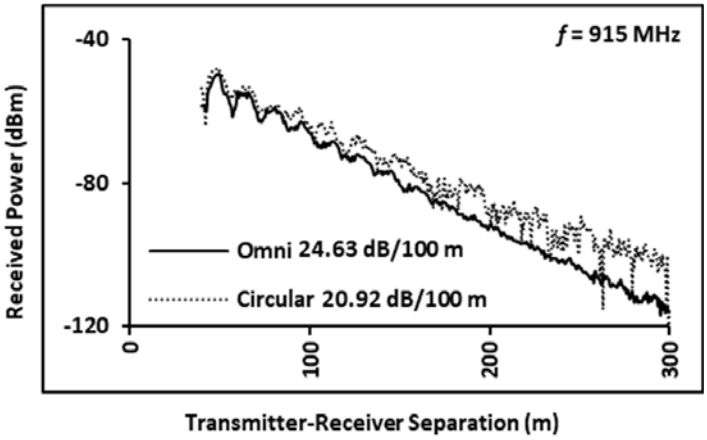

Figure 11. Influence of circular polarization.

considerable influence on RF propagation in smaller-dimension tunnels with significant height to width ratios.

This influence was most notable in Grand Coulee Dam's 900 Gallery at 915 MHz. The propagation slope for the circularly polarized signal showed a 3-dB/100 m improvement over the horizontally polarized signal (Fig. 11).

The circular Tx antenna's cross polarization-isolation was essentially unity, allowing equal amounts of vertical and horizontal polarized RF signal to be transmitted as compared to the omnidirectional Tx antenna, which transmitted primarily in horizontal polarization. Again, due to the height to width ratio, the 900 Gallery favored vertically polarized signal propagation and the Rx antenna received more vertically polarized RF signal from the circular Tx antenna than from the omnidirectional Tx antenna, resulting in a lower attenuation slope value.

Similar to the signal attenuation slope, signal gains were estimated using a method of linear regression fitting from a point well beyond the near zone — 20 m for 455 MHz, 40 m for 915 and 2450 MHz, and 80 m for 5800 MHz — to the end of the far zone of measured RF propagation for each frequency, antenna, and polarization combination. Using the linear regression fit's y intercepts, signal gain differences were then calculated for similar frequency, antenna, and polarization combinations using the omnidirectional antenna at each frequency and polarization as a reference. Gain calculations were completed only if the differences in attenuation slopes between the two signals were less than 1.5 dB. Fig. 9 shows the result of the calculation of signal gain for the Yagi antenna at 2450 MHz.

Signal gain estimates support the ray tracing modeling prediction that antenna pattern typically does not significantly influence behavior in the far zone except for a constant gain offset. However, signal gains did not typically match the antenna gain specified by the vendor and varied between environments and polarizations as shown in Table 3. (See Section 6 for a full discussion of the data in Table 3.)

6. SUMMARY

Data for the influence of antenna pattern on RF signal propagation in the far zone are summarized in Tables 2 and 3. Specific antenna polarizations are indicated by TxV/C-RxV and TxH/C-RxH, where Tx is the transmit antenna and Rx is the receive antenna. Polarizations follow three designations based on orientation: V for vertical, H for horizontal, and C for circular. For example, "TxH/C-RxH" would indicate that the transmit antenna was either linear horizontal or circular polarized — based on the antenna type used — and the receive antenna was linear horizontal polarized. Antenna polarizations oriented for favored RF signal propagations based on tunnel dimensions are shown in Tables 2 and 3 with shaded backgrounds [2, 10, 14].

Signal attenuation slope data in Table 2 are presented in two formats: estimated slope loss in

Table 3. Summary of estimated RF propagation signal gain.

Frequency/ Far Zone	Antenna Parameters			Grand Coulee Dam	Western Coal Mine	Experimental Mine
	Pol.	Type	Relative Gain (dB)	Gain (dB)	Gain (dB)	Gain (dB)
455 MHz > 20 m	TxV-RxV	Omni	Ref	Ref	Ref	Ref
		Yagi	9.15	4.06	9.26	n/a
	TxH-RxH	Omni	Ref	Ref	Ref	Ref
		Yagi	9.15	n/a	9.83	8.57
915 MHz > 40 m	TxV/C-RxV	Omni	Ref	Ref	Ref	Ref
		Yagi	9.05	6.47	8.27	6.08
		Patch	5.85	5.10	5.36	5.15
		Circular	5.85	-0.97	1.88	n/a
	TxH/C-RxH	Omni	Ref	Ref	Ref	Ref
		Yagi	9.05	9.38	6.71	6.81
		Patch	5.85	9.01	5.99	5.56
		Circular	5.85	n/a	6.21	5.59
2450 MHz > 40 m	TxV/C-RxV	Omni	Ref	Ref	Ref	Ref
		Yagi	9.5	12.16	12.73	11.45
		Patch	3.0	4.23	5.96	3.80
		Circular	3.0	3.17	2.04	2.44
	TxH/C-RxH	Omni	Ref	Ref	Ref	Ref
		Yagi	9.5	13.40	11.37	11.50
		Patch	3.0	5.45	4.33	3.40
		Circular	3.0	3.83	n/a	-9.53
5800 MHz > 80 m	TxV/C-RxV	Omni	Ref	Ref	Ref	Ref
		Yagi	8.5	10.40	2.69	10.57
		Patch	1.5	-1.91	n/a	-1.33
		Circular	1.5	-1.37	n/a	-2.63
	TxH/C-RxH	Omni	Ref	Ref	Ref	Ref
		Yagi	8.5	3.45	-0.40	16.81
		Patch	1.5	-9.41	-9.21	7.53
		Circular	1.5	No data	No data	No data

dB/100 m for each frequency, polarization, and antenna combination, and slope difference for like antennas referenced to an omnidirectional antenna at the same frequency and polarization. With the exceptions outlined in the Results and Discussion section, the data show an antenna's pattern has very little influence on RF signal propagation attenuation slope in the far zone of propagation in tunnels. For linear polarized antennas, differences in attenuation slope for like frequencies, antennas, and polarizations typically varied by less than 1.5 dB.

Table 3 presents signal gain data for each frequency, polarization, and antenna combination as referenced to an omnidirectional antenna. As discussed in the Results and Discussion section, gain was only calculated when the attenuation slopes between antennas differed by less than 1.5 dB. The 5800 MHz circular polarized antenna developed a high level of insertion loss at some point between the measurements made at Grand Coulee Dam and the high-seam coal mine. This resulted in an overall lower signal level, thus negating any attempts to estimate signal gains. It is important to note that a higher level of insertion loss would not influence attenuation slope estimates.

The measurement results also once again confirmed the influences of frequency, antenna polarization, and tunnel dimensions on RF signal propagation [2, 10, 14]. This influence was most pronounced at 455 and 915 MHz in the smaller dimensions of Grand Coulee Dam's 900 Gallery and Bruceton Experimental Mine's Main entry.

7. CONCLUSION

The influence of antennas on radio signal propagation in tunnels and underground mining environments is quite different from that on the surface and has not been well understood. Starting with a simple concrete tunnel and progressing to the complex environment of underground mines, extensive measurements were made to study the influence of antenna pattern and polarization on radio signal propagation. The tunnels and mines surveyed in this study include a gallery in a concrete dam, a typical high-seam coal mine, and a small experimental coal mine.

The results show that in the near zone of propagation, change in signal strength is affected strongly by the antenna and has a complex character. In the far zone of propagation, signal strength is generally uniform with respect to attenuation slope and antenna gain.

Understanding the influence of antenna pattern on radio signal propagation is a key element in designing reliable wireless systems, which are critical to production and miner safety and health in underground mines.

ACKNOWLEDGMENT

The authors wish to acknowledge the management and staff of the United States Bureau of Reclamation's Grand Coulee Dam for its cooperation and assistance in this work. The authors would also like to thank Nick Damiano, General Engineer, NIOSH Pittsburgh Mining Research Division (PMRD), for his assistance in making the measurements.

DISCLAIMER

The findings and conclusions in this report are those of the authors and do not necessarily represent the official position of the National Institute for Occupational Safety and Health, Centers for Disease Control and Prevention. Mention of any company or product does not constitute endorsement by the National Institute for Occupational Safety and Health, Centers for Disease Control and Prevention.

REFERENCES

1. Mahmoud, S. F. and J. R. Wait, "Geometrical optical approach for electromagnetic wave propagation in rectangular mine tunnels," *Radio Science*, Vol. 9, 1147–1158, 1974.
2. Emslie, A., R. Lagace, and P. Strong, "Theory of the propagation of UHF radio waves in coal mine tunnels," *IEEE Transactions on Antennas and Propagation*, Vol. 23, 192–205, 1975.
3. Chiba, J., T. Inaba, Y. Kuwamoto, O. Banno, and R. Sato, "Radio communication in tunnels," *IEEE Transactions on Microwave Theory and Techniques*, Vol. 26, No. 6, 439–443, 1978.
4. Zhang, Y. P., Z. R. Jiang, T. S. Ng, and J. H. Sheng, "Measurements of the propagation of UHF radio waves on an underground railway train," *IEEE Transactions on Vehicular Technology*, Vol. 49, No. 4, 1342–1347, 2000.
5. Didascalou, D., J. Maurer, and W. Wiesbeck, "Subway tunnel guided electromagnetic wave propagation at mobile communications frequencies," *IEEE Transactions on Antennas and Propagation*, Vol. 49, No. 11, 1590–1596, 2001.
6. Wang, T. S. and C. F. Yang, "Simulations and measurements of wave propagations in curved road tunnels for signals from GSM base stations," *IEEE Transactions on Antennas and Propagation*, Vol. 54, No. 9, 2577–2584, 2006.
7. Molina-Garcia-Pardo, J. M., M. Lienard, A. Nasr, and P. Degauque, "On the possibility of interpreting field variations and polarization in arched tunnels using a model for propagation in rectangular or circular tunnels," *IEEE Transactions on Antennas and Propagation*, Vol. 56, No. 4, 1206–1211, 2008.
8. Masson, E., P. Combeau, M. Berbineau, R. Vauzelle, and Y. Pousset, "Radio wave propagation in arched cross section tunnels-simulations and measurements," *Journal of Communication*, Vol. 4, No. 4, 276–283, 2009.

9. Lienard, M. and P. Degauque, "Natural wave propagation in mine environments," *IEEE Transactions on Antennas and Propagation*, Vol. 48, 1326–1339, 2000.
10. Zhou, C., T. Plass, R. Jacksha, and J. A. Waynert, "RF propagation in mines and tunnels: Extensive measurements for vertically, horizontally, and cross-polarized signals in mines and tunnels," *IEEE Antennas and Propagation Magazine*, Vol. 57, No. 4, 88–102, 2015.
11. Goddard, A. E., "Radio propagation measurements in coal mines at UHF and VHF," *Proceedings: Through-the-Earth Electromagnetics Workshop*, 15–17, Aug. 1973.
12. Boutin, M., A. Benzakour, C. L. Despins, and S. Affes, "Radio wave characterization and modeling in underground mine tunnels," *IEEE Transactions on Antennas and Propagation*, Vol. 56, No. 2, 540–549, 2008.
13. Jacksha, R., C. Zhou, and C. Sunderman, "Measurement of the influence of antenna pattern on radio frequency propagation in a concrete tunnel," *2018 IEEE Radio and Wireless Symposium (RWS)*, 103–105, 2018.
14. Zhou, C., J. Waynert, T. Plass, and R. Jacksha, "Attenuation constants of radio waves in lossy-walled rectangular waveguides," *Progress In Electromagnetics Research*, Vol. 142, 75–105, 2013.
15. Balanis, C. A., *Advanced Engineering Electromagnetics*, John Wiley & Sons, 1999.
16. Dudley, D. G., M. Lienard, S. F. Mahmoud, and P. Degauque, "Wireless propagation in tunnels," *IEEE Antennas and Propagation Magazine*, Vol. 49, No. 2, 11–26, 2007.
17. Alonso, J., B. Izquierdo, and J. Romeu, "Break point analysis and modelling in subway tunnels," *3rd European Conference on Antennas and Propagation, 2009, EuCAP 2009*, 3254–3258, IEEE, Mar. 2009.
18. Guan, K., Z. Zhong, B. Ai, and C. Briso-Rodríguez, "Research of propagation characteristics of break point: Near zone and far zone under operational subway condition," *Proceedings of the 6th International Wireless Communications and Mobile Computing Conference*, 114–118, ACM, Jun. 2010.
19. Zhang, Y. P., "Enhancement of waveguide model for propagation-loss prediction in tunnels," *Microwave and Optical Technology Letters*, Vol. 30, No. 1, 10–12, 2001.
20. Klemenschits, T. and E. Bonek, "Radio coverage of road tunnels at 900 and 1800 MHz by discrete antennas," *5th IEEE International Symposium on Personal, Indoor and Mobile Radio Communications, 1994, Wireless Networks-Catching the Mobile Future*, Vol. 2, 411–415, IEEE, Sep. 1994.
21. Watson, P. A. and M. Arbabi, "Crosspolarisation isolation and discrimination," *Electronics Letters*, Vol. 9, No. 22, 516–517, 1973.
22. Balanis, C., *Antenna Theory Analysis and Design*, 3rd Edition, A John Wiley & Sons, Inc., Publication, 2005.
23. Kraus, J. D. and R. J. Marhefka, *Antennas for All Applications*, 3rd Edition, McGraw-Hill Science, 2001.